Hydrophobic-Region-Induced Transitions in Self-Assembled Peptide Nanostructures†

Hai Xu,*,‡ Jing Wang,‡ Shuyi Han,‡ Jiqian Wang,‡ Daoyong Yu,‡ Hongyu Zhang,§ Daohong Xia,‡ Xiubo Zhao,|| Thomas A. Waigh,|| and Jian R. Lu*,||

Centre for Bioengineering and Biotechnology and School of Chemistry and Chemical Engineering, China University of Petroleum (East China), 66 Changjiang West Road, Qingdao Economic Development Zone, Qingdao 266555, China, and Biological Physics, School of Physics and Astronomy, University of Manchester, Schuster Building, Manchester M13 9PL, U.K.

Received August 10, 2008. Revised Manuscript Received November 15, 2008

Peptide amphiphiles readily self-assemble into a variety of nanostructures, but how molecular architectures affect the size and shape of the nanoaggregates formed is not well understood. From a combined TEM and AFM study of a series of cationic peptide surfactants A_mK (m = 3, 6, and 9), we show that structural transitions (sheets, fibers/worm-like micelles, and short rods) can be induced by increasing the length of the hydrophobic peptide region. The trend can be interpreted using the molecular packing theory developed to describe surfactant structural transitions, but the entropic gain, decreased CAC, and increased electrostatic interaction associated with increasing the peptide hydrophobic chain need to be taken into account appropriately. Our analysis indicates that the trend in structural transitions observed from A_mK peptide surfactants is opposite to that obtained from conventional monovalent ionic surfactants. The outcome reflects the dominant role of hydrophobic interaction between the side chains opposed by backbone hydrogen bonding and electrostatic repulsion between lysine side chains.

Introduction

As a promising approach to fabricating novel materials and devices on the nanoscale, short peptide self-assembly has been extensively explored over the past few decades. The inspiration for the development of advanced materials through molecular self-assembly is drawn from biology, where many biomolecules, including nucleic acids, polysaccharides, phospholipids, polypeptides, and proteins, interact and self-organize to form well-defined structures that are strongly correlated with their resultant functionalities.[1] The self-assembly process is driven by weak noncovalent interactions, including hydrogen bonding, van der Waals forces, electrostatic interactions, hydrophobicity, and stacking effects. Although these interactions may be relatively insignificant in isolation, when combined, they are sufficient to generate well-ordered supramolecular structures.

To date, many short peptides have been reported to self-assemble efficiently into various nanostructures, including fibers, tapes, tubes, and spheres. Ghadiri and co-workers were among the first to demonstrate the production of peptide-based nanotubes.[2,3] These authors showed that small cyclic peptides with an even number of alternating L- and D-amino acid residues can self-assemble into an array of nanotubular structures through hydrogen bonding. Gazit et al. reported that the diphenylalanine peptide, the core recognition motif of the Alzheimer's β-amyloid polypeptide, can efficiently self-assemble into long, hollow tubular nanostructures with remarkable rigidity.[4,5] Their later studies revealed that the noncharged peptide analogue (Ac-Phe-Phe-NH_2) and other aromatic homodipeptides such as diphenylglycine and dipara-iodo-Phe can also form well-ordered nanostructures, all showing the significance of the stacking of aromatic moieties on the order and directionality of the assemblies.[6,7] Stupp and co-workers developed peptide amphiphiles consisting of a hydrophobic alkyl tail and a single hydrophilic peptide motif.[8,9] They found that these peptide amphiphiles can self-assemble from aqueous media into nanofibrous networks through pH changes or divalent ion induction. In parallel, Matsui et al. have also developed another family of peptide amphiphiles—bolaamphiphiles, where two hydrophilic peptides were conjugated through a hydrophobic alkyl chain.[10] They reported that bis(*N*-α-amido-glycylglycine)-1,7-heptane dicarboxylate self-assembled into tubular nanostructures under acidic conditions and the intermolecular hydrogen bonds were proposed to dictate the assembly mechanism. Studies by Zhang et al. and others recently demonstrated that surfactant-like peptides self-assembled into ordered nanoscale structures in bulk soluton[11−13] and at interfaces.[14,15] These surfactant-like peptides typically included seven to eight residues consisting of at least one charged amino acid

† Part of the Neutron Reflectivity special issue.

* Corresponding authors. Phone: 86-532-86981569 (H.X.), 44-161-2003926 (J.R.L.). E-mail: xuh@upc.edu.cn (H.X.), j.lu@manchester.ac.uk (J.R.L.).

‡ Centre for Bioengineering and Biotechnology, China University of Petroleum (East China).

§ School of Chemistry and Chemical Engineering, China University of Petroleum (East China).

|| University of Manchester.

(1) Whitesides, G. M.; Mathias, J. P.; Seto, C. T. *Science* **1991**, *254*, 1312–1319.

(2) Ghadiri, M. R.; Granja, J. R.; Milligan, R. A.; McRee, D. E.; Khazanovich, N. *Nature* **1993**, *366*, 324–327.

(3) Ghadiri, M. R.; Granja, J. R.; Buehler, L. K. *Nature* **1994**, *369*, 301–304.

(4) Reches, M.; Gazit, E. *Science* **2003**, *300*, 625–627.

(5) Kol, N.; Adler-Abramovich, L.; Barlam, D.; Shneck, R. Z.; Gazit, E.; Rousso, I. *Nano Lett.* **2005**, *5*, 1343–1346.

(6) Reches, M.; Gazit, E. *Isr. J. Chem.* **2005**, *45*, 363–371.

(7) Reches, M.; Gazit, E. *Nano Lett.* **2004**, *4*, 581–585.

(8) Hartgerink, J. D.; Beniash, E.; Stupp, S. I. *Science* **2001**, *294*, 1684–1688.

(9) Hartgerink, J. D.; Beniash, E.; Stupp, S. I. *Proc. Natl. Acad. Sci. U.S.A.* **2002**, *99*, 5133–5138.

(10) Matsui, H.; Gologan, B. *J. Phys. Chem. B* **2000**, *104*, 3383–3386.

(11) Vauthey, S.; Santoso, S.; Gong, H.; Watson, N.; Zhang, S. *Proc. Natl. Acad. Sci. U.S.A.* **2002**, *99*, 5355–5360.

(12) Santoso, S.; Hwang, W.; Hartman, H.; Zhang, S. *Nano Lett.* **2002**, *2*, 687–691.

(13) von Maltzahn, G.; Vauthey, S.; Santoso, S.; Zhang, S. *Langmuir* **2003**, *19*, 4332–4337.

(14) Lu, J. R.; Perumal, S.; Powers, E. T.; Kelly, J. W.; Webster, J. R. P.; Penfold, J. *J. Am. Chem. Soc.* **2003**, *125*, 3751–3757.

(15) Lu, J. R.; Perumal, S.; Hopkinson, I.; Webster, J. R. P.; Penfold, J.; Hwang, W.; Zhang, S. *J. Am. Chem. Soc.* **2004**, *126*, 8940–8947.

10.1021/la802499n CCC: $40.75
Published on Web 12/29/2008

such as aspartic acid and lysine at their hydrophilic heads and a string of hydrophobic amino acids (termed the hydrophobic region to distinguish it from the alkyl tail in alkyl peptides) such as alanine, valine, and leucine at their tails. When dissolved in water under neutral pH conditions, these peptides self-assembled into ordered nanotubes and vesicles.

Because of their unique features such as biocompatibility and facile chemical and biological modifications, peptide-based self-assembled nanostructures have found applications in (1) the delivery of drugs, genes, and proteins where peptide nanostructures act as carriers via encapsulation or electrostatic interaction,[16] (2) tissue engineering where peptides self-assemble to generate 3D networks of nanostructures that serve as a scaffold for cell culture,[17,18] and (3) electronic and biomimetic mineralization where the self-assembled peptide nanostructures are used as templates to induce the nucleation, growth, and alignment of nanocrystals, thereby resulting in the formation of metallic nanowires made from silver, nickel or copper, and other highly ordered superstructures of minerals or composites such as hollow silica nanotubes, CdS nanofibers, and hydroxylapatite.[4,8,19−21] Recent work has shown that peptides can also facilitate the solubilization and crystallization of several membrane proteins such as glycerol-3-phosphate dehydrogenase (GlpD), rhodopsin, and photosystem I without causing any structural damage or loss of activities.[22−24] Because normal surfactants cannot dissolve membrane proteins, peptide surfactants may accelerate the study of the structure of membrane proteins. The fiber phases of peptide surfactants are analogous to wormlike micellar solutions in conventional ionic surfactants, whose unusual viscoelasticities find many applications in the delivery of home care products (solution structuring in shampoos, creams, and detergents).[25]

In spite of extensive studies and the great potential of self-assembled peptide surfactants, it is still unclear as to how to link their molecular architecture to their morphology on the nanometer scale. This primarily stems from the diversity of the 20 naturally occurring and countless de novo amino acid residues that differ in size, shape, charge, polarity, and hydrophobicity. The combination of these residues is enormous, not only resulting in the vast variation of basic building blocks but also making it difficult to manipulate the subsequent driving forces of molecular self-assembly. As a result, it is often impossible to rationalize the different contributions involved in a given system. To circumvent this problem, we designed a model system that enables the self-assembly of peptide surfactants to be controlled in a systematic manner as a function of the hydrophobic peptide region. No other systematic studies have been previously reported for full peptide surfactants to assess the structural effect arising from their hydrophobic region length.

Experimental Section

Chemicals. Protected amino acids (Fmoc-Ala-OH and Fmoc-Lys(Boc)-OH), *O*-(1H-benzotriazole-1-yl)-*N*,*N*,*N*′,*N*′-tetramethyluronium hexafluorophosphate (HBTU), *N*-hydroxybenzotriazole anhydrous (HOBt anhydrous), *N*,*N*′-diisopropyl ethylamine (DIEA), and rink amide MBHA resin were purchased from GL Biochem (Shanghai) Ltd. and used as received. Other regents and solvents were obtained from Sigma and used without further purification unless otherwise stated. Dichloromethane (DCM) and dimethyl formamide (DMF) were redistilled and subsequently dried with molecular sieves prior to use. All water used was from a Millipore water purification system with a minimum resistivity of 18.0 MΩ·cm.

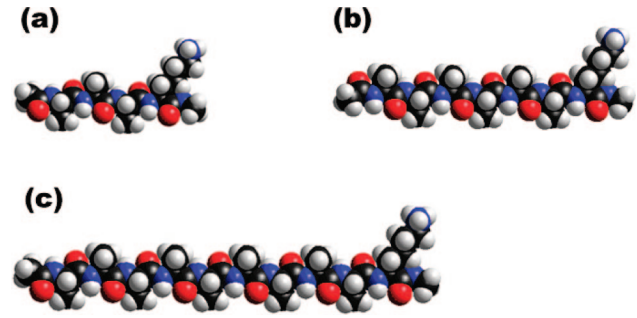

Figure 1. Molecular structures of (a) A_3K, (b) A_6K, and (c) A_9K. The full lengths of these molecules have been calculated to be 1.7, 2.7, and 3.7 nm, respectively. The K residue is located on the right (C terminal) in each sequence, with each molecule carrying one positive charge. Color scheme: carbon (black), hydrogen (white), oxygen (red), and nitrogen (blue).

Synthesis of Peptide Surfactants. A series of cationic surfactant peptides was synthesized with one lysine residue at the C terminus as the hydrophilic head and with three to nine consecutive alanine residues as the hydrophobic tail (Figure 1) using the standard Fmoc solid-phase synthesis from natural L-amino acids.[11−13] The C terminus was amidated, and the N terminus was acetylated, thus generating one positive charge per molecule (from the lysine residue side chain) at neutral pH. The peptides had purities of well over 98% from reverse-phase HPLC and mass spectrometry (Figures SI-1 and SI-2). Peptide synthesis was performed on a CEM Liberty microwave peptide synthesizer, where microwave energy was utilized to drive deprotection, coupling, and cleavage reactions. Owing to reducing chain aggregation, the utilization of microwaves increased the reaction rates and helped improve product purity. All peptides were synthesized from Rink-amide resin using standard Fmoc solid-phase synthesis techniques. The use of Rink-amide resin was to provide C-terminally amidated peptides. After the deprotection of Rink-amide resin with a 20% piperidine and 0.1 M HoBt in DMF solution, Fmoc-Lys(Boc)-OH was introduced and coupled with resin, followed by Fmoc deprotection and coupling with Fmoc-Ala-OH. The cycle of Fmoc deprotection and coupling with Fmoc-Ala-OH was repeated until the designed peptide sequences were obtained. After Fmoc deprotection of the N-terminal residue, the N terminus was capped with acetic anhydride. All coupling reactions (including acetylation) were affected by treatment with HBTU/HOBt/DIEA. Cleavage and Boc deprotection of the side chain of the lysine residue was performed with a mixture of triflouroacetic acid, triisopropylsilane, H_2O, and ethanedithiol in a ratio of 94:1:2.5:2.5. The cleavage mixture and two subsequent DCM washings were filtered into a round-bottomed flask and rotary evaporated to a concentrated solution that was subsequently dropped into cold ethyl ether for precipitation. The ether solution was centrifuged for 20 min at 4 °C and 10000 rpm. The solid product was collected, washed with a copious amount of ether, and lyophilized for 2 days before purification analysis by reverse-phase HPLC and mass spectrometry.

The lyophilized peptides were dissolved in Milli-Q water to create solutions with a peptide concentration of 3 mM, and the solution pH was found to be around 6 (minor pH adjustments were made by using HCl or NaOH with ionic strengths kept constant at around 2 mM). The peptide solutions were then filtered through a 0.22 μm filter and sonicated in a water bath for 10 min. The resultant clear solutions were stored for 1 week at room temperature prior to TEM and AFM characterizations.

(16) Yan, X.; He, Q.; Wang, K.; Duan, L.; Cui, Y.; Li, J. *Angew. Chem., Int. Ed.* **2007**, *46*, 2431–2434.
(17) Silva, G. A.; Czeisler, C.; Niece, K. L.; Beniash, E.; Harrington, D. A.; Kessler, J. A.; Stupp, S. I. *Science* **2004**, *303*, 1352–1355.
(18) Mahler, A.; Reches, M.; Rechter, M.; Cohen, S.; Gazit, E. *Adv. Mater.* **2006**, *18*, 1365–1370.
(19) Matsui, H.; Pan, S.; Gologn, B.; Jonas, S. H. *J. Phys. Chem. B* **2000**, *104*, 9576–9579.
(20) Yuwono, V. M.; Hartgerink, J. D. *Langmuir* **2007**, *23*, 5033–5038.
(21) Stone, E. D.; Stupp, S. I. *J. Am. Chem. Soc.* **2004**, *126*, 12756–12757.
(22) Kiley, P.; Zhao, X.; Vaughn, M.; Baldo, M. A.; Bruce, B. D.; Zhang, S. *PLoS Biol.* **2005**, *3*, 1180–1186.
(23) Zhao, X.; Zhang, S. *Chem. Soc. Rev.* **2006**, *35*, 1105–1110.
(24) Zhao, X.; Nagai, Y.; Reeves, P.; Kiley, P.; Khorana, H. G.; Zhang, S. *Proc. Natl. Acad. Sci. U.S.A.* **2006**, *103*, 17707–17712.
(25) Driess, C. A. *Soft Matter* **2007**, *3*, 956–970.

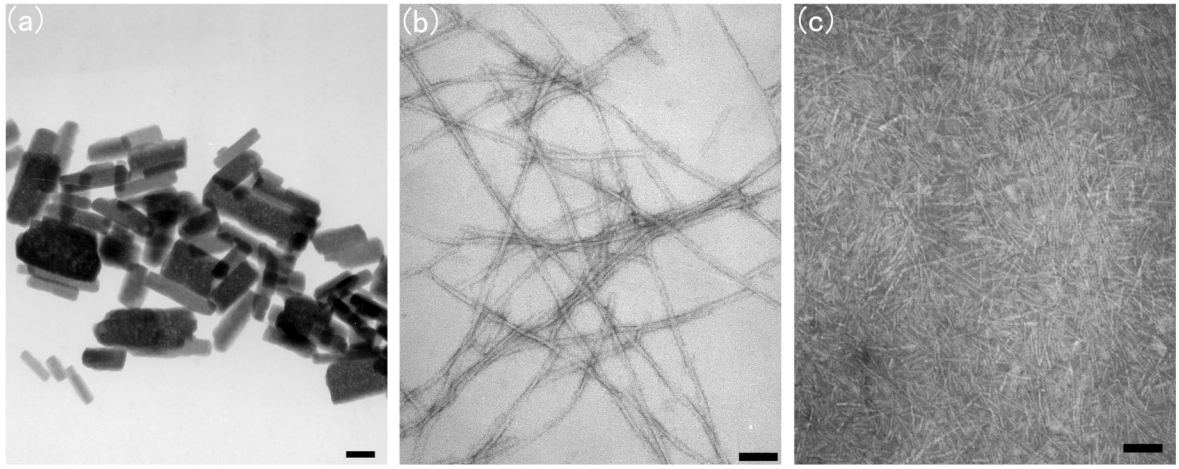

Figure 2. TEM micrographs of assemblies of (a) A_3K, (b) A_6K, and (c) A_9K. (The scale bar represents 50 nm.) All samples were prepared by dissolution in water at a concentration of 3 mM and the solution pH was adjusted to 6.0. Prior to TEM characterization, the peptide solutions were stored at least for 1 week. Samples were negatively stained with uranyl acetate.

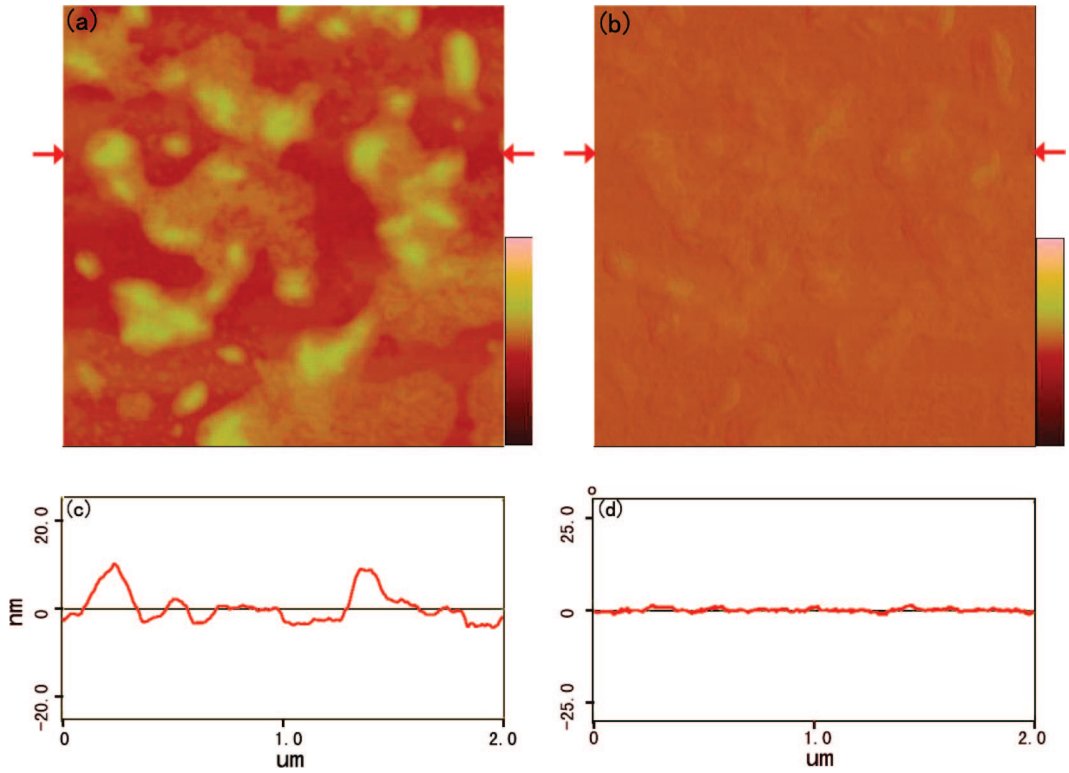

Figure 3. (a) Height AFM image (1 μm × 1 μm) of A_3K assemblies (3 mM at pH 6.0) and (b) the corresponding phase image. The z scales are 50 nm and 60° for the height and phase images, respectively, all being shown to the right of the images. (c) The typical height section profile showing the distinguished height variation along the line scan indicated by the red arrows in image a, and (d) the typical phase section profile showing little phase variation along the line scan indicated by the red arrows in image b.

Transmission Electron Microscopy. TEM sample preparation was done on the basis of the method described by Gazit et al.[4−7] Samples were placed on a 400 mesh copper grid covered by carbon-stabilized Formvar film. After 2 min, excess fluid was removed, and the grid was negatively stained with 2% (w/v) uranyl acetate in water. The samples were viewed using a JEOL 1200EX electron microscope operated at 80 kV. Care was taken not to dry the sample excessively so that the images reflect the self-assembly onto the surface from an aqueous environment. For a given peptide sample, the TEM images were taken from two independently prepared samples to ensure reproducibility and avoid artifacts.

Atomic Force Microscopy. AFM measurements were performed with a commercial Nanoscope IVa MultiMode AFM (Digital Instruments, Santa Barbara, CA) in tapping mode. Topographic (height) and phase images were recorded concurrently under ambient conditions. All samples were probed with a TESP silicon probe (Veeco, Santa Barbara, CA) having a nominal spring constant of 42 N/m and a typical frequency of 300 kHz. Samples were prepared by dropping 10 μL of peptide solutions onto freshly cleaved mica surfaces. After 30 s, the mica surfaces were rinsed extensively with water and dried gently with nitrogen gas. Care was again taken not to over dry the samples. To prevent impurity adsorption on the prepared surface, AFM characterization was performed immediately after all traces of water had disappeared (usually within 2 min). Images were collected at a scan rate of 1 Hz and at a scan angle of 0°. All images are flattened using a first-order line fit (the flatten function in AFM software) to correct for piezo-derived differences between scan lines. Measurements were made at least three times

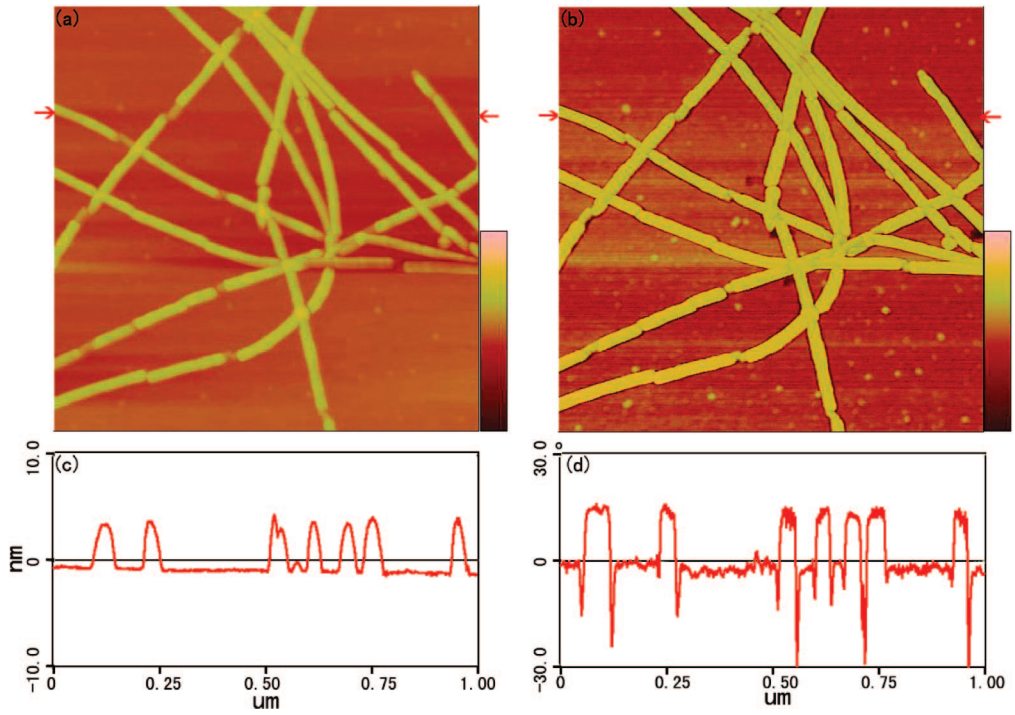

Figure 4. (a) Height AFM image (1 μm × 1 μm) of A_6K assemblies (3 mM at pH 6.0) and (b) the corresponding phase image. The z scales are 20 nm and 60° for the height and phase images, respectively, with both being shown to the right of the images. (c) The typical height section profile shows the distinguished height variation along the line sca indicated by the red arrows in image a, and (d) the typical phase section profile also shows obvious phase variation along the line scan indicated by the red arrows in image b.

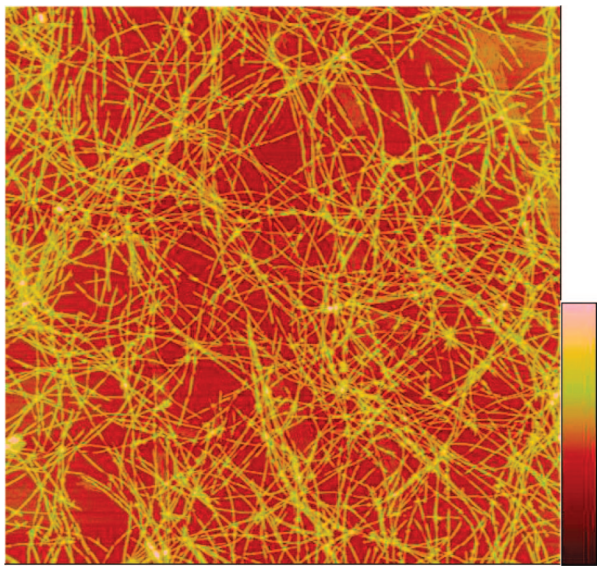

Figure 5. Low-magnification height AFM image of A_6K assembled nanofibers (3 mM at pH 6.0). The scan size is 5 μm × 5 μm, and the z scale is 20 nm, as shown to the right of the image.

in each case in the middle area of the sample, and representative images are shown here.

FTIR. Infrared spectra of the three peptide solutions were measured by means of a Nicolet 6700 FT-IR spectrometer equipped with a DTGS detector. To avoid interference from the solvent H_2O that exhibits strong adsorption near 1640 cm^{-1} that overlaps with the amide I band of peptides, an ARK HATR accessory equipped (Thermal Electron) with a ZnSe crystal and a trough sampling plate was used in our IR measurements. The ATR technique produced a less intense solvent contribution to the overall infrared spectrum, so the solvent can be more readily subtracted from the sample spectrum of interest. The spectra were recorded at room temperature from 4000 to 400 cm^{-1}, and 64 scans were collected with a spectral resolution of 2 cm^{-1}. Reference spectra were recorded under identical conditions in moisturized air.

Results and Discussion

The basic molecular structures of the peptide surfactants as shown in Figure 1 are analogous to common surfactants such as sodium dodecyl sulfate (SDS) having one charged amino acid at one end, followed by several consecutive hydrophobic amino acids (hydrophobic region). By varying only the number of alanine residues, the effect of the length of the hydrophobic region on the supramolecular structures through the self-assembly of peptide surfactants in aqueous solution has been examined by atomic force microscopy (AFM) and transmission electron microscopy (TEM). These studies have revealed interesting variations in the size and shape of the self-assembled nanostructures, and the results are shown in Figures 2 and 3; membrane sheets are formed from A_3K, long nanofibers (worm-like micelles) are formed from A_6K, and short nanorods are formed from A_9K. We have rationalized this structural evolution with respect to the hydrophobic region length by comparison with the behavior of normal hydrocarbon surfactants. This work is essential for the development of a predictive model to link molecular architectures with self-assembled nanostructures, leading to the effective tuning of peptide self-assembly.

TEM. We first show the negatively stained TEM images taken from all three peptides with the strikingly different nanostructures presented in Figure 2. The A_6K peptide formed thin fibrillar morphologies (worm-like micelles, Figure 2b). These nanofibers were quite uniform with a diameter of 8.0 ± 1 nm. They appear to be fairly flexible (persistence length ~100 s nm), have high axial ratios, and can elongate to several micrometers to form a network of non-cross-linked nanofibers. Thus, A_6K provides an example of a worm-like micellar solution with semidilute polymeric liquid viscoelastic properties (no yield stress, which also indicates no cross-links). A_9K TEM imaging revealed the

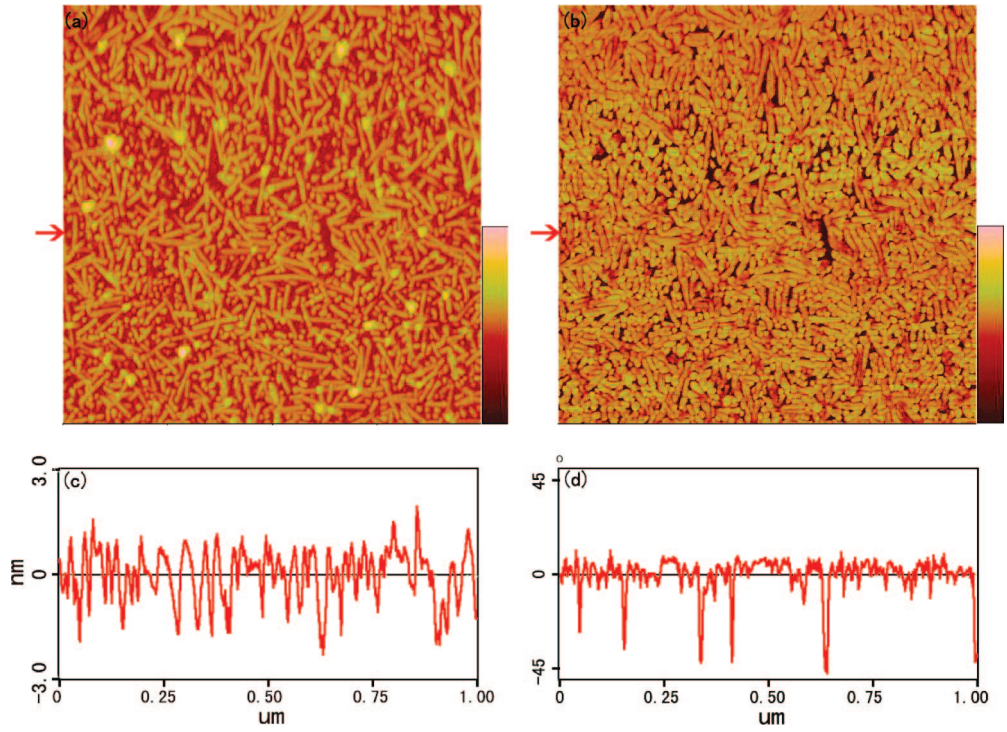

Figure 6. (a) 1 μm × 1 μm height AFM image of A_9K assemblies (3 mM at pH 6.0) and (b) the corresponding phase image. The z scales are 10 nm and 60° for the height and phase images, respectively, with both being shown to the right of the images. (c) The typical height section profile showing the distinguished height variation along the line scan as indicated by the red arrow in image a, and (d) the typical phase section profile showing obvious phase variation along the line scan as indicated by the red arrow in image b.

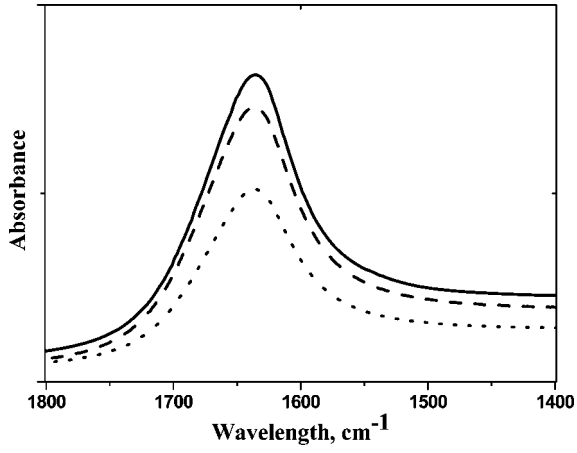

Figure 7. Amide I region of ATR FTIR spectra from the three peptide solutions at pH 6.0 and a peptide concentration of 3 mM: A_3K, dotted line; A_6K, dashed line; and A_9K, solid line.

formation of thin and short nanorods. As shown in Figure 2c, their diameters are about 3.0 ± 1 nm, and their lengths do not exceed 100 nm. The conditions used for TEM imaging closely mimicked those used for solution assembly instead of for dried peptide samples. Uranyl acetate was employed as an aqueous negative stain, and care was taken to follow the same sample treatments so that good reproducibility of the TEM images was obtained.

In contrast to the fibrillar nanostructures, the TEM image from A_3K (Figure 2a) revealed the formation of sheets. These plate-like structures appeared to be symmetrical with clear borders but were unstable during the TEM measurement. The instability could arise from the formation of lamellar stacks of A_3K molecules that were sensitive to dehydration under the vacuum TEM measurement conditions. In contrast, the assemblies of A_6K and A_9K were relatively stable, and few changes in morphology were observed during the measurements, possibly because of their higher hydrophobicity that caused tighter packing of the hydrophobic region in aqueous solution.

Through the combined study of electrical conductivity, AFM, and spectroscopic ellipsometry, the critical aggregation concentration (CAC) of A_6K in water was found to be around 0.2 mM, which is slightly lower than the previously reported value of 1 mM from dynamic light scattering.[26] The CAC for A_9K was around 0.015 mM. A_3K did not exhibit a distinct CAC in the concentration range from 0.01 to 10 mM studied. Instead, surface tension measurements for this peptide displayed a gradual decrease in surface tension with increasing concentration. Thus, as the hydrophobic peptide chain increased, the CAC decreased, and the peptides started to aggregate at lower peptide concentrations. The size and shape of the assembled nano-objects changed with hydrophobic peptide region length. As already described above, A_3K formed stacked bilayers; A_6K formed long fibers; aggregates of A_9K followed the same trend as A_6K, but their diameter and length were significantly reduced.

All of the peptide assemblies described above were produced at around pH 6.0. When the solution pH was adjusted to above 11.0, no characteristic supramolecular structures were formed, but instead irregular clumps were observed by TEM. Each peptide surfactant had a single side chain amino group of lysine with a pK_a value of around pH 10. As the pH approached the pK_a, the head groups became deprotonated, eliminating the electrostatic repulsion among the head groups and lowering their solubility. These changes transformed the self-assembled nanostructures to amorphous morphologies. The transition reflected the delicate balance of the charge interaction associated with peptide surfactant head groups, and the effect is broadly similar to the trend observed for peptides bearing alkyl chain tails reported by Stupp et al.[17,21]

(26) Nagai, A.; Nagai, Y.; Qu, H.; Zhang, S. *J. Nanosci. Nanotechnol.* **2007**, *7*, 1–7.

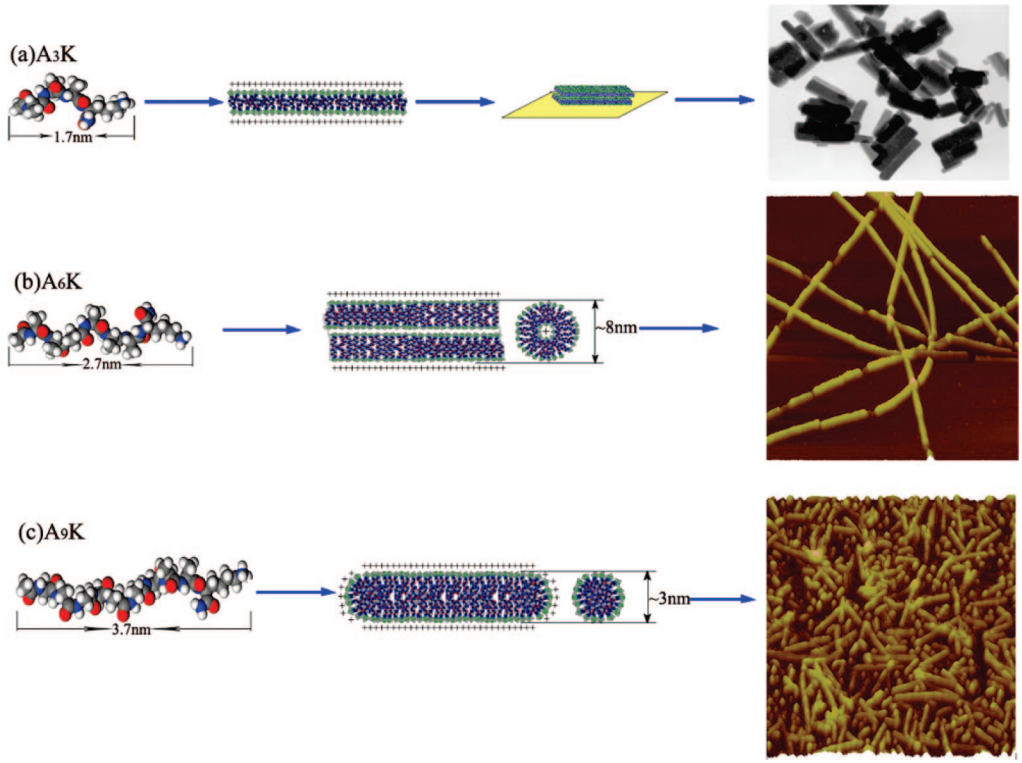

Figure 8. Schematic illustration of peptide surfactant self-assembly. (a) A_3K has the shortest chain and has no apparent CAC detected, giving rise to the lowest effective a_e and the highest packing parameter; consequently, stacked A_3K bilayers are formed. (b)With increasing hydrophobic tail length and decreasing CAC of A_6K, the electrostatic repulsion between the head groups increases. This, together with the packing and entropic effect, leads to the lowering of the packing parameter and the formation of nanofibers. (c) A_9K has the lowest CAC, the highest electrostatic repulsion between head groups, and the largest entropic effect arising from the longest tail, resulting in the lowest p and the formation of nanorods. In each case, lysine (K) groups remain at the outer surface of the nanostructures formed.

AFM. AFM offered a useful alternative to TEM for confirming the structural features formed from peptide surfactants, and it avoided the sophisticated sample preparation required in TEM. In the AFM study, peptide solution was deposited on a clean mica surface, and the adsorption was allowed to proceed for 1 min before the surface was rinsed with pure buffer and then dried gently under a weak stream of nitrogen. We found that this drying process helped to remove any excess water but retained water hydration within peptide self-assembled nanostructures. The surface was then imaged using tapping mode in an ambient environment. Both topographical and phase images were recorded concurrently. The presence of A_3K patches was again revealed in the topographical image and was consistent with the TEM study (Figure 3). However, these sheets covered large areas and were more irregular than those observed under TEM. The difference could arise from the surface chemistry used (TEM copper grid versus mica in AFM) and the different extents of dehydration related to different sample environments. However, the AFM phase image showed no obvious contrast, indicating full surface coverage by the A_3K lamellae and good structural and mechanical homogeneity.

The topographical and phase images for the nanostructures formed from A_6K were also obtained, along with their corresponding sectional profiles (Figure 4). These images exhibit the prevalent morphology of nanofibers, consistent with TEM analysis. The lateral dimensions measured directly by AFM were rather exaggerated because of the convolution of the AFM tip with the sample. However, the vertical displacement of the AFM cantilever was not affected by the convolution. Thus, the vertical dimension gave a more accurate determination of the height.[27] The height profile (Figure 4c) revealed an average value of 5.0 $\pm$ 1.0 nm as compared to the diameter of 8.0 $\pm$ 1.0 nm from the TEM analysis. The reduction most likely resulted from some degree of deformation of nanofibrils caused by the compression of the AFM tip. Such deformation is very common in the AFM characterization of soft matter systems such as proteins, DNA, and peptides, even if tapping mode is employed.[28,29] The lateral nominal diameter from the AFM section analysis was found to be some 25 $\pm$ 3 nm and was strongly dependent on the tip diameter. The persistence length of the worm-like micelles of A_6K in AFM measurements is on the order of 100 s nm, in agreement with TEM techniques.

Unlike that in A_3K, there is a strong phase contrast in A_6K nanofibers, as evident from Figure 4b. The corresponding sectional profile is shown in Figure 4d. Although the assignment of bright and dark contrast to the soft or hard material is not always straightforward, the bright region in Figure 4b is easily attributed to peptide nanofibers when compared with the corresponding height image as shown in Figure 4c. The sectional analysis from the phase image (Figure 4d) provides a steeper inclination near the edges of the nanofibers than that obtained from the topographical image (Figure 4c). Thus, the phase sectional profile would provide a better characterization of diameter and width of the nanofibers although the latter requires a careful characterization of the AFM tip diameter.

(27) Kuznetsov, Y. G.; Malkin, A. J.; Lucas, R. W.; Plomp, M.; McPherson, A. *J. Gen. Virol.* **2001**, *82*, 2025–2034.
(28) Toscano, A.; Santore, M. M. *Langmuir* **2006**, *22*, 2588–2597.
(29) Margeat, E.; Grimellec, C. L.; Royer, C. A. *Biophys. J.* **1998**, *75*, 2712–2770.

Both AFM height and phase images as shown in Figure 4a,b reveal the formation of long A_6K nanofibers from short ones containing small gaps and joints. The lengths of these short nanofibers vary, but their diameters are almost constant. Each long, uniform nanofiber might be formed through an annealing process in which the short ones were aligned. Further AFM measurements revealed that the alignment was slow and occurred over a period of hours. In addition, micelles or vesicular sheets were also present, and they could be better viewed from the phase image. The kinetic pathway of the molecular self-assembly could then involve the initial formation of micelles/vesicular sheets that were then fused into short nanofibers. The short nanofibers subsequently underwent interconnections to form longer nanofibers, similar to the feature reported by Gale et al.[30] From a low-magnification AFM image of A_6K assemblies, the occurrence of some nanofibrillar overlapping or networking in excess of 1 μm is easily seen (Figure 5). The extent of their interaction at the overlapping points will have direct implications on solution viscoelastic properties as indicated previously.

The topographical and phase images of A_9K nanostructures, along with their corresponding sectional profiles, are reproduced in Figure 6. Apart from the nanorods, many spherical micelles/vesicular sheets are also visible across the AFM image. The height section profile by AFM revealed that the diameters of the nanorods and micelles were consistent with those of nanorods obtained from TEM, 3.0 ± 1 nm. The better consistency of the microscopic measurements on A_9K reflects the greater rigidity of the nanorods that must arise from the longer hydrophobic region length and denser packing.

Infrared Measurements. Apart from the hydrophobic interaction, hydrogen bonding together with the electrostatic repulsion between lysine side chains also plays a significant role in peptide nanostructuring. Hydrogen bonding arising from the backbone structuring influences IR absorption, transition frequencies, and extinction coefficients.[32,33] The amide I region originating from the amide carbonyl stretching frequencies between approximately 1600 and 1700 cm^{-1} is often used to assess the amide modes. Amide groups in β-pleated sheets give rise to useful diagnostic bands within the amide I region. As noted previously, great care had been taken to ensure that the AFM and TEM imaging analyses revealed the peptide self-assembly in the hydrated state, thereby presenting a close reflection of solution nanostructuring. From the ATR-FTIR study of the peptide aqueous solution, it was revealed that all peptide surfactant solutions exhibited a strong amide I band around 1635 cm^{-1}, indicating that all of the aggregated nanostructures adopted a predominantly β-sheet structure (Figure 7). This result is consistent with other IR studies from similar peptide amphiphiles[34−36] upon self-assembly. The formation of β-sheet structure is characteristic of peptide chain packing within different nanostructures, including nanofibers and nanotubes constructed by the intermolecular assembly of peptide amphiphiles,[34−36] amphiphilic β-hairpin peptides,[37] and truncated β-amyloid peptides.[38,40] Lamm et al.[37] reported β-sheet formation between peptide backbones of $(VK)_4$-VPPT-$(KV)_4$, and growth, driven by intermolecular hydrogen bonding, was achieved along the fibrillar axis to over micrometers in length. Paramonov et al.[35] reported that for the self-assembly of peptide amphiphiles consisting of 19 *N*-methylated variants and 7 alanine mutants, β-sheet hydrogen bonding was critically important in driving the process into nanofibers; otherwise, only spherical micelles comprising the inner hydrophobic core and the outer hydrophilic peptide shell would occur. Dong et al.[39] have also reported an ABA block motif where the central B block is composed of alternating hydrophilic and hydrophobic amino acids (glutamine and leucine, respectively) to favor β-sheet conformation through intermolecular backbone hydrogen bonding, leading to infinite fiber growth in aqueous solution. Block A consists of several positively charged lysine residues whose electrostatic repulsion at neutral pH works against the fibrous assembly of the B block. They showed that by balancing the sizes of block A against B, fully soluble nanofibers with different diameter and length were formed. Their systems, which are different from ours, have shown how the size of stacking hydrogen bonding units are balanced against the interaction from the head groups' counterbalancing assembly, resulting in changes in the size and shape of the nanostructures formed. Clearly, hydrogen bonding between peptide backbones is important in our systems, but the similarity between the infrared spectra may imply that the structural transitions are driven by the increasing hydrophobic interaction with the peptide region length.

Interfacial Packing and Shape Transition. Although Stupp et al. and others[34−40] have elegantly described the structural transitions for different peptide series by the interplay between backbone hydrogen bonding, hydrophobic interaction between the side chains, and electrostatic repulsion between the charged amino acid head groups, the molecular architectures that have been reported are diversified, and it remains difficult to attempt to make any quantitative description of the relative contributions from each interaction involved. Our work to be described below represents a very preliminary effort to rationalize the different aspects of the contributions involved.

The concept of a molecular packing parameter is widely used to predict the size and shape of surfactant aggregates formed in aqueous solution.[41] Because the peptide surfactants studied in our work broadly resemble the main structural feature of alkyl surfactants, we explore how structural transition theory is used in the peptide surfactant system. We note that although both types of surfactants bear the same amphiphilic structure character the hydrophobic peptide region is distinctly different from a simple hydrocarbon tail. Nevertheless, it remains attractive to explore to what extent this concept could be used to rationalize the structural transition of the peptide surfactants.

Following the extensive studies by Tanford,[31] Israelachvili et al.,[41] and Nagarajan,[42,43] the molecular packing parameter p is defined as

(30) Gale, M.; Pollanen, M. S.; Martiewicz, P.; Goh, M. C. *Biophysical J.* **1995**, *68*, 2124.
(31) Tanford, C. *The Hydrophobic Effect*; Wiley: New York, 1973.
(32) Mansa, E. S.; Getahun, A.; Wright, W. W.; DeGrado, W. F.; Vanderkooi, J. M. *J. Am. Chem. Soc.* **2000**, *122*, 9883–9888.
(33) Surewicz, W. K.; Mantsch, H. H.; Chapman, D. *Biochemistry* **1993**, *32*, 389–394.
(34) Niece, K. L.; Hartgerink, J. D.; Donners, J. J. J. M.; Stupp, S. I. *J. Am. Chem. Soc.* **2003**, *125*, 7146–7147.
(35) Paramonov, S.E.; Jum; H, W.; Hartgerink, D. *J. Am. Chem. Soc.* **2006**, *128*, 7291–7298.
(36) Jiang, H.; Guler, M. O.; Stupp, S. I. *Soft Matter* **2007**, *3*, 454–462.
(37) Lamm, M. S.; Rajagopal, K.; Schneider, J. P.; Pochan, D. J. *J. Am. Chem. Soc.* **2005**, *127*, 16692–16700.
(38) Burkoth, T. S.; Benzinger, T. L. S.; Urban, V.; Morgan, D. M.; Gregory, D. M.; Thiyagarajan, P.; Botto, R. E.; Meredith, S. C.; Lynn, D. G. *J. Am. Chem. Soc.* **2002**, *120*, 7883–7889.
(39) Dong, H.; Paramonov, S. E.; Aulisa, L.; Bakota, E. L.; Hartgerink, J. D. *J. Am. Chem. Soc.* **2007**, *129*, 12468–12472.
(40) Lu, K.; Jacob, J.; Thiyagarajan, P.; Conticello, V. P.; Lynn, D. G. *J. Am. Chem. Soc.* **2003**, *125*, 6391–6393.
(41) Israelachvili, J.; Mitchell, D. J.; Ninham, B. W. *J. Chem. Soc., Faraday Trans. 2* **1976**, *72*, 1525–1568.
(42) Nagarajan, R.; Ruckenstein, E. *Langmuir* **1991**, *7*, 2934–2969.
(43) Nagarajan, R. *Langmuir* **2002**, *18*, 31–38.

$$p = \frac{a_o}{a_e} \quad (1)$$

where a_o is the cross-sectional area of the tail and a_e is the equilibrium area occupied by each surfactant at the curved interface in the aggregate. It is widely observed experimentally that for many surfactant systems with $0 \le p \le 1/3$, spherical micelles form; with $1/3 \le p \le 1/2$, cylindrical micelles form; and with $1/2 \le p \le 1$, bilayer or lamellar sheets form. Therefore, if the packing parameter is known, then the size and shape of the equilibrium aggregates can be predicted.

However, more subtle effects due to the hydrophobic tail length are not included in this analysis. The equilibrium a_e depends on the strength of the repulsive interaction (α) and the surface free energy (σ), but we also need to account for the free energy of chain stretching in their particular morphology. Following the analysis of Nagarajan,[42,43] we introduce the equation

$$a_e = \left(\frac{\alpha}{\sigma} + \frac{2Q/a_e}{\sigma/kT}\right)^{1/2} \quad (2)$$

where Q depends on the tail length (it is inversely proportional to the tail length) and aggregate shape and kT is the thermal energy.

The structural transition with respect to the length of the hydrophobic peptide region is schematically summarized in Figure 8. Under the conditions studied, A_3K, A_6K, and A_9K carry one positive charge (K) on each molecule. For simplicity, we assume that their basic amphiphilic feature resembles an ionic surfactant. For a monovalent ionic surfactant in aqueous solution, the molecular packing parameter predicts a decrease in the spontaneous curvature (H_0) of the surfactant monolayer with increasing alkyl chain length, equivalent to an increase in the size of the micellar aggregates.[44] Given that this simple geometrical approach should be used with care (peptide surfactants are structurally different), it may be clearly observed that an increase in the length of the hydrophobic tail from A_3 to A_6 transformed the peptide surfactant morphology from stacked lamellae to cylindrical nanofibers. A further increase in the hydrophobic region to A_9K caused a substantial reduction in the length and diameter of the nanofibers. The resultant nanorods for A_9K had well-defined end caps on both ends. The gradual transition from stacked bilayers to long cylinders and finally to short end-capped nanorods corresponded to a gradual increase in spontaneous curvature, opposite to the trend predicted for monovalent ionic surfactants. As will be described in the following text, in spite of this apparent inconsistency, the structural transition based on the molecular packing parameter proposed by Tanford[31] and Israelachvili et al.[41] from surfactant research can still be used to rationalize the peptide surfactant aggregation.

Two significant assumptions are often made in predicting the transition of aggregate geometries: (1) a_e is dominated by the cross-sectional area of the surfactant head and (2) the length of the alkyl tail has little effect on the packing and structural transitions. However, a_e not only is a simple geometrical property of the headgroup but also is controlled by the equilibrium free energy of the system.[43] In fact, a_e is primarily dependent on headgroup interaction parameter α as shown in eq 2. Furthermore, although a_0 is often assumed to be independent of tail chain length (n_c), the actual contribution of n_c can be significant, depending on the precise shape of the surfactant aggregates formed ($Q \approx 1/n_c$ in eq 2). Nagarajan has recently extended Tanford's free-energy expression to account for the packing entropy contribution of the surfactant tails to aggregates.[43] The solution of eq 2 shows that the hydrophobic tail directly influences the equilibrium area (a_e), and this area increases with hydrophobic chain length. Thus, the packing parameter p in eq 1 decreases with increasing hydrophobic chain length, giving the correct trend for the size and shape of the peptide surfactant aggregates formed. The CACs follow the conventional ordering with an increased tail group size, decreasing the free-energy change for micellization and thus increasing its propensity (it dominates this property, i.e., a higher n_c) provides a lower CAC.

The structural transition with respect to the length of the hydrophobic peptide chain in the corresponding bulk solutions for these peptides has not yet been studied in this work. However, a number of recent studies by Zhang et al.[11−13] have examined the solution nanostructures of A_6K and its homologue with the same hydrophobic tail length using TEM. The samples were prepared through the quick-freeze/deep-etch procedure to minimize possible changes in solution aggregate structure during the fast freezing process. These studies revealed that A_6K and its homologue V_6K formed similar aggregated structures consisting of both nanofibers and vesicles. The bulk solutions contained more irregular sizes and shapes of aggregates that were not observed from our surface measurements. Moreover, the nanofiber diameters varied over a much wider range, although most of them were between 30 and 50 nm with the nanofiber lengths being about 1000 nm, consistent with the dimensions estimated from dynamic light scattering. The coexistence of different sizes and shapes of aggregates was indicative of the dynamic aggregation process and also reflected the energy barriers associated with the equilibration. It was found from this characterization work that it took more than 24 h for the aggregation to reach the equilibrated state. During the first few hours, the surface-bound aggregates showed a more diversified variation in size and shape, similar to the observations reported by Zhang et al.

It thus appears that during the early stage of peptide assembly various smaller nano-objects formed that then gradually further assembled into larger nano-objects. The eventual formation of long nanofibers in the bulk solution from A_6K was entirely consistent with what was observed at the mica surface from AFM. Furthermore, the mature fiber lengths were also similar, as was also revealed from our TEM work. However, the diameters were rather different. The diameters of our surface-bound A6K nanofibers were between 5 and 8 nm and were much narrower. The difference might arise from different solution conditions (peptide concentration and ionic strength) used. The interaction with solid surfaces could also contribute to the observed difference.

Conclusions

Our AFM and TEM results show an interesting structural transition caused by the increase in the hydrophobic peptide region in the peptide surfactant systems that were studied. Whereas both lamellar sheets and nanofibers are reminiscent of the action of intermolecular hydrogen bonding, the structural transition strongly suggests the increasing effect of hydrophobic interaction between the hydrophobic tails. An increase in the hydrophobic peptide tail length imposes a direct influence on packing within peptide nanostructures and the CAC of the self-assembly process. The trend in the variation in the size and shape of peptide aggregates can be accounted for using the packing parameter concept widely used for common surfactants, but the contribution of the entropic free energy of the hydrophobic tails needs to be taken into account.

Understanding the relationship between molecular architecture and the geometry of nanostructures formed is important for the

(44) Bergström, L. M. *J. Colloid Interface Sci.* **2006**, *293*, 181–193.

exploitation of the potential of peptide surfactants in technological applications. The present study provides a useful rationalization toward this goal. Further experimental work to include more peptide surfactants (e.g., A_4K, $A_{12}K$, $A_{15}K$) in this series will help strengthen the proposed structural transition as reported here and add credibility to the development of reliable theoretical analysis to this surfactant series.

Acknowledgment. This work was supported by the National Natural Science Foundation of China under grant no. 20773164 and the UK Engineering and Physical Science Research Council (EPSRC). We acknowledge helpful discussions with Dr. Robert K. Thomas at Oxford University and Dr. Shuguang Zhang at MIT.

Supporting Information Available: HPLC profiles, MALDI-TOF MS analysis, and calculated molecular masses of A_3K, A_6K, and A_9K. This material is available free of charge via the Internet at http://pubs.acs.org.

LA802499N